Published OnlineFirst May 29, 2013; DOI: 10.1158/0008-5472.CAN-13-0109

Tumor and Stem Cell Biology

Cancer Research

Chromatin Regulator PRC2 Is a Key Regulator of Epigenetic Plasticity in Glioblastoma

Atsushi Natsume[1], Motokazu Ito[1,2], Keisuke Katsushima[2], Fumiharu Ohka[2], Akira Hatanaka[2], Keiko Shinjo[2], Shinya Sato[4], Satoru Takahashi[4], Yuta Ishikawa[5], Ichiro Takeuchi[5], Hiroki Shimogawa[7], Motonari Uesugi[7], Hideyuki Okano[8], Seung U. Kim[10,11], Toshihiko Wakabayashi[1], Jean-Pierre J. Issa[12], Yoshitaka Sekido[3,6], and Yutaka Kondo[2,3,9]

Abstract

Tumor cell plasticity contributes to functional and morphologic heterogeneity. To uncover the underlying mechanisms of this plasticity, we examined glioma stem-like cells (GSC) where we found that the biologic interconversion between GSCs and differentiated non-GSCs is functionally plastic and accompanied by gain or loss of polycomb repressive complex 2 (PRC2), a complex that modifies chromatin structure. PRC2 mediates lysine 27 trimethylation on histone H3 and in GSC it affected pluripotency or development-associated genes (e.g., *Nanog*, *Wnt1*, and *BMP5*) together with alterations in the subcellular localization of EZH2, a catalytic component of PRC2. Intriguingly, exogenous expression of EZH2-dNLS, which lacks nuclear localization sequence, impaired the repression of *Nanog* expression under differentiation conditions. RNA interference (RNAi)–mediated attenuation or pharmacologic inhibition of EZH2 had little to no effect on apoptosis or bromodeoxyuridine incorporation in GSCs, but it disrupted morphologic interconversion and impaired GSC integration into the brain tissue, thereby improving survival of GSC-bearing mice. Pathologic analysis of human glioma specimens revealed that the number of tumor cells with nuclear EZH2 is larger around tumor vessels and the invasive front, suggesting that nuclear EZH2 may help reprogram tumor cells in close proximity to this microenvironment. Our results indicate that epigenetic regulation by PRC2 is a key mediator of tumor cell plasticity, which is required for the adaptation of glioblastoma cells to their microenvironment. Thus, PRC2-targeted therapy may reduce tumor cell plasticity and tumor heterogeneity, offering a new paradigm for glioma treatment. *Cancer Res; 73(14); 4559–70. ©2013 AACR.*

Introduction

Cancers are mostly composed of heterogeneous cell populations. A significant degree of morphologic and lineage heterogeneity may contribute to tumor expansion, invasion, metastasis, and drug resistance (1). These multiple distinct subpopulations of cancer cells within tumors may derive from a limited source of cancer cells, called cancer stem cells (CSC), which may have plasticity and respond to signals from their microenvironment (1–3). Such stem-like cancer cells have been well characterized in glioblastoma multiforme, and are referred to as glioma stem-like cell (GSC; refs. 4–7). These cells are considered to be capable of aberrantly differentiating into diverse cell types in response to oncogenic cues. Although CSCs can differentiate into non-CSCs, the reverse process is now also being considered (8, 9). This phenotypic plasticity between CSCs and non-CSCs may be regulated by signals within the tumor microenvironment.

Alongside known genetic changes, aberrant epigenetic alterations have emerged as common hallmarks of many cancers including glioblastoma (10–12). Epigenetic silencing in cancer cells is mediated by at least two mechanisms, namely polycomb repressive complex 2 (PRC2)–mediated histone H3 lysine 27 trimethylation (H3K27me3) and DNA methylation–mediated gene silencing, the latter of which is closely associated with H3K9 di- or tri-methylation (H3K9me2/3; refs. 13–15). A significant difference between the two mechanisms centers on the stability of transcriptional repression; H3K27me3-mediated gene silencing can change dynamically as opposed to DNA methylation within CpG islands, which

Authors' Affiliations: [1]Department of Neurosurgery, Nagoya University School of Medicine; Divisions of [2]Epigenomics and [3]Molecular Oncology, Aichi Cancer Center Research Institute; [4]Department of Experimental Pathology and Tumor Biology, Nagoya City University Graduate School of Medical Sciences; [5]Department of Scientific and Engineering Simulation, Graduate School of Engineering, Nagoya Institute of Technology; [6]Department of Cancer Genetics, Nagoya University Graduate School of Medicine, Nagoya; [7]Institute for Integrated Cell-Material Sciences/Institute for Chemical Research, Kyoto University, Kyoto; [8]Department of Physiology, Keio University School of Medicine; [9]Precursory Research for Embryonic Science and Technology (PRESTO), Japan Science and Technology Agency, Tokyo, Japan; [10]Division of Neurology, Department of Medicine, University of British Columbia, Vancouver, Canada; [11]Medical Research Institute, Chungang University College of Medicine, Seoul, Republic of Korea; and [12]Fels Institute for Cancer Research and Molecular Biology, Temple University, Philadelphia, Pennsylvania

Note: Supplementary data for this article are available at Cancer Research Online (http://cancerres.aacrjournals.org/).

A. Natsume and M. Ito contributed equally to this work.

Corresponding Author: Yutaka Kondo, Division of Epigenomics, Aichi Cancer Center Research Institute, 1-1 Kanokoden, Chikusa-ku, Nagoya 464-8681, Japan. Phone: 81-52-764-2994; Fax: 81-52-764-2994; E-mail: ykondo@aichi-cc.jp

doi: 10.1158/0008-5472.CAN-13-0109

Published OnlineFirst May 29, 2013; DOI: 10.1158/0008-5472.CAN-13-0109

is highly stable without artificially altering key factors in the cells (16).

In vertebrates, PRC2-mediated H3K27me3 processes confer stemness and control organism development by regulating the expression of developmental genes during embryonic development (17–19). In particular, a recent study showed that deletion of the histone methyltransferase of PRC2, Ezh2, in mice changes the balance between differentiation and self-renewal of cortical progenitor cells, thus altering the rates of neurogenesis and developmental timing (20). Given the roles of PRC2-mediated H3K27me3 during development, plastic and dynamic interconversion between CSCs and non-CSCs may also be associated with PRC2-mediated H3K27me3 epigenetic process.

In this context, using glioblastoma as a highly heterogeneous tumor model, we investigated the PRC2-mediated H3K27me3 mechanism that regulate the interconversion between GSCs and non-GSCs, which may be a key process involved in the cancer phenotype including formation of tissue heterogeneity. Our study also provides evidence that support tumor cell plasticity as a potential therapeutic target against human gliomas.

Materials and Methods

Primary tumors, establishment of glioma-initiating cells, and human neural stem cells

Glioma tissue samples were obtained from 3 patients (# 1228, 0316, and 0125) undergoing surgical treatment at the Nagoya University Hospital (Nagoya, Japan), after they provided written informed consent. The procedures used for derivation of GSCs were described previously (21, 22). Serum-induced brain tumor cells (S-BTC) were established by culturing GSCs in Dulbecco's Modified Eagle Medium (Invitrogen) containing FBS. We examined different concentrations of FBS (0.1%, 1%, and 10%) and found that even low concentrations of serum (0.1% and 1%) still showed the same morphologic conversion as with 10% serum, although the effects were less stable. Therefore, we used 10% serum as reported previously (5). A human neural stem cell (NSC) line, namely HB1.F3, was generated from the human fetal telencephalon as described previously (23). GFP coding sequence was ligated into the multiple cloning site of pLNCX2 retrovirus vector (TAKARA). Virus containing the pLNCX2-GFP construct was used to infect 1228-GSC and 0316-GSC lines according to a previously reported protocol (15). GSC lines (1228, 0316, and 0125) stably expressing the GFP under the *Nestin* promoter using pE/nestin:EGFP construct (GSC-pE-Nes) were also generated (24). About the EZH2 exogenous expression, a hemagglutinin (HA)-tagged short hairpin RNA (shRNA)–insensitive EZH2 expression construct (EZH2-exp) was generated by PCR-based site-directed mutagenesis to create CATG*C*AG*G*CA*A*GT*T*TA*C*GA (five mutated residues are shown in italic font) and cloned into pcDNA3-mRFP vector (13032; Addgene). We also modified this EZH2-exp construct and generated shRNA-insensitive EZH2 lacking nuclear localization signal (NLS; deletion of 491–495 amino acids of EZH2, which correspond to the NLS; ref. 25).

Antibodies

Anti-β-tubulin (Tuj-1; Millipore), anti-GFAP (Z0334; DAKO), anti-human Nestin (MAB1259; R&D Systems), anti-Nanog (9092; Cell Signaling Technology), anti-EZH2 (AC22; Cell Signaling Technology), anti-SUZ12 (37375; Cell Signaling Technology), anti-EED (05-1320; Millipore), and anti-CD133 (130-190-422; Miltenyi Biotec) were used for immunocytochemistry. Rabbit anti-human EZH2 (36-6300; Zymed), mouse anti-EZH2 (AC22), mouse monoclonal anti-human glial fibrillary acidic protein (GFAP; M0761; DAKO), and rabbit polyclonal anti-human Nestin (AB5922; Millipore) were used for immunohistochemistry. Antibodies against EZH2 (AC22; Cell Signaling Technology), K27 trimethylated histone H3 (07-449; Millipore), anti-histone H3 (ab1791; Abcam), inhibitor of IκB kinase α (IKKα; sc-7182; Santa Cruz Biotechnology), and β-actin (BH10D10; Cell Signaling Technology) were used for immunoblotting.

Sphere formation assay in 96-well plates

GSCs were converted into S-BTCs after 3 weeks of continuous exposure to serum. S-BTCs were trypsinized and placed into 96-well plates (50 cells/well) in NBE media with N2 and B27 supplements, basic fibroblast growth factor (bFGF), and EGF, as described earlier. Seven days after seeding, spheres were counted (each sphere contained more than 10 cells). The rate of sphere formation was then calculated by (the number of spheres/the number of cells seeded) × 100. On average, 51.1% ± 11.3% (1228-S-BTC) and 57.9% ± 10.2% (0316-S-BTC) of the cells reformed spheres.

3-Deazaneplanocin A treatment of cells

3-Deazaneplanocin A (DZNep) was synthesized from a commercially available cyclopentenone derivative (CAS: 163317-01-9; CHEMSTEP) as described elsewhere (26). Spectroscopic data of the synthesized DZNep were identical to those used in a previous study (26).

RNA interference

Retroviral vectors were designed [RNA interference (RNAi)-Ready pSIREN-RetroQ Vector; Clontech Laboratories] encoding a shRNA directed against EZH2 (target sequences of 5′-CATGTAGACAGGTGTATGA-3′, Ver. C or 5′-ATATGACTGCTTCCTACAT-3′, Ver. B; ref. 15) or directed against WNT1 (target sequences of 5′-CATCGAATCCTGCACGTGT-3′, Ver. 1 or 5′-CCACGAACCUGCUUACAGA-3′, Ver. 2). A detailed protocol was described previously (15). Cells were incubated with viruses [multiplicity of infection (MOI) = 0.4] in the presence of retronectin (40 μg/mL; TAKARA). Both constructs could reduce *EZH2* or *Wnt1* expression around 70% to 80%. For control purposes, we used an shRNA vector targeting luciferase (Luc; synthesized by BD Biosciences) and an empty vector (mock).

Transfection of the *BMP5* gene

A retrovirus vector was manipulated (pLNCX2; Clontech Laboratories) to encode full-length *BMP5* (accession number, NM_021073). The target vector was cotransfected with pVSV-G (TAKARA) into GP2-293 cells (TAKARA) and virus-containing medium obtained according to the manufacturer's protocol.

Published OnlineFirst May 29, 2013; DOI: 10.1158/0008-5472.CAN-13-0109

Real-time PCR analyses

Total RNA was isolated using TRIzol (Invitrogen), and 2 μg was reverse transcribed with Superscript Reverse Transcriptase (Invitrogen). TaqMan or SYBR Green quantitative PCR (qPCR) was then conducted in duplicate for the target genes, with the oligonucleotide primers used shown in Supplementary Table S1. Relative values to glyceraldehyde-3-phosphate dehydrogenase (GAPDH) expression were used for normalization.

RNA expression microarray and data analysis

Targets for microarray hybridization were generated from RNA according to the manufacturer's instructions (Agilent Technologies). Whole Human Genome Microarrays (Agilent Technologies), were used for gene expression profiling. In each array, unreliable probes (identified using the same protocol as GeneSpring software; Agilent Technologies) were considered as missing-values in the following statistical analysis. The expression level signals were $\log_2$-transformed and normalized, so that the ($\log_2$-transformed) expression levels of each array had zero mean and unit variance. Pearson correlation coefficient and its statistical significance were computed. Principal component analysis (PCA) was applied to expression data obtained from each analysis.

Chromatin immunoprecipitation

Chromatin immunoprecipitation (ChIP) assays were conducted on the basis of a modification of previously published methods (13). The lysate was incubated with either 10 μL of anti-K4 dimethylated histone H3 (07-030; Millipore), anti-K27 trimethylated histone H3 (07-449; Millipore), or anti-histone H3 (ab1791; Abcam) antibody. An aliquot (2%) of total lysate was incubated with 10 μL TE buffer [10 mmol/L Tris (pH 8.0) and 1 mmol/L EDTA] at 4°C overnight as a negative control. Because the number of GSCs was limited, we needed to increase the signal and reduce the background of ChIP. The amount of antibody was optimized for each modification to get the maximum amount of DNA while keeping the signal-to-noise ratio high. We used a magnetic bead system to reduce the loss of material during the washing step (10003D; Life Technologies). To minimize the loss of DNA, we used conventional phenol chloroform DNA extraction instead of column extraction system. ChIP products were used for confirmation ChIP-PCR, with the relevant oligonucleotide primers shown in Supplementary Table S1. TaqMan or SYBR Green qPCR was conducted in an ABI Prism 7000 (Applied Biosystems) in triplicate for the target genes.

ChIP-microarray analyses

We analyzed ChIP products as probes on the 88K promoter array (G4475A; Agilent Technologies). A detailed protocol for ChIP-microarray (ChIP-chip) was described previously (13, 15). Results were analyzed by the neighborhood error model in ChIP Analytics software; a probe X was considered "bound" if $P(X) < 0.05$ and at least one neighboring probe had $P(X) < 0.1$ (version 1.1; Agilent Technologies). After probes were identified by the software, probes with signal ratio (target/input) for each target gene >2.0 were further selected. The data of our microarray analysis are available in the Array express (http://www.ebi.ac.uk/arrayexpress) with accession code: E-TABM-1121.

Methylated CpG island amplification-microarray

Global analysis using methylated CpG island amplification-microarray (MCAM) technology was carried out using DNA from the cell lines and normal brain tissue as described previously (27–29). The data of our microarray analysis are available in the Array express (http://www.ebi.ac.uk/arrayexpress) with accession codes: E-TABM-1122.

Bisulfite pyrosequencing methylation analysis

We conducted bisulfite treatment as reported previously (29). Primer sequences and conditions used for methylation determination are shown in Supplementary Table S1. The methylation levels at three CpG sites were averaged to represent the degree of methylation for the *Nanog* gene.

Cell growth assay

GSCs (1×10^4) were plated in 12-well culture dishes for 24 hours before DZNep treatment (5 or 10 μmol/L). GSCs were treated with DZNep or PBS (control) for 72 hours and transferred to NBE media without DZNep. Cell numbers were determined every 3 days. Experiments were carried out independently in triplicate.

Bromodeoxyuridine incorporation assay

Bromodeoxyuridine (BrdUrd) incorporation was assessed using a FACSCalibur apparatus (Becton Dickinson) according to the manufacturer's instructions.

Animal experiments

Animal experiments were carried out according to the principles described in the Guide for the Care and Use of Laboratory Animals prepared by the Office of the Prime Minister of Japan. We stereotactically injected GSCs or S-BTCs resuspended in 5 μL PBS into 5- to 6-week-old nonobese diabetic/severe combined immunodeficient (NOD/SCID) female mice (SLC). Four weeks after the GFP-expressing GSCs (1228- and 0316-GSC-GFP) were inoculated in the brain of NOD/SCID mice, the presence of GFP-expressing tumors was confirmed by an *in vivo* spectral imaging system (Maestro2; CRi). On the same day, mice bearing GFP-expressing gliomas were injected with DZNep (50 μg) or PBS (control) via single intratumoral (i.t.) injection route. Another 4 weeks after the initiation of treatment, the presence of tumors was determined by biofluorescence imaging. Furthermore, the survival time was evaluated by the Kaplan–Meier method.

Brain slice model

The brains of female BALB/c nude mice were cut into 300-μm coronal slices by a vibratome (VT 1000 E; Leica), which were transferred onto 30-mm Millicell-CM inserts (pore size, 0.4 mm; Millipore) in 6-well culture plates. EZH2-shRNA-, BMP5-expressing-, or Wnt1-shRNA–transduced GSC spheres or control GSC spheres were placed onto the brain slices. After 7-day culture, the slice was fixed with 4% paraformaldehyde and immunostained with mouse monoclonal anti-human GFAP (M0761; DAKO) and rabbit polyclonal anti-human Nestin (AB5922; Millipore) antibodies. The fluorescent areas were quantified with the Developer Toolbox 1.7 software (GE Healthcare).

Published OnlineFirst May 29, 2013; DOI: 10.1158/0008-5472.CAN-13-0109

Results

Characterization of GSCs from human glioblastoma

We established GSC lines (1228-, 0316-, and 0125-GSCs) that were capable of reproducibly forming tumors in the brain of NOD/SCID mice even with 10^2 cells and were serially transplantable (Supplementary Table S2). The expression of *CD133*, *Nestin*, and *Nanog*, as CSC markers or pluripotency-related markers, was positive in the majority of cell lines (Fig. 1A and Supplementary Fig. S1A). Genome-wide expression profiles of 0316- and 1228-GSCs were similar to each other and resembled the ones obtained with NSCs, whereas gene expression profiles of the parental glioblastoma tumors were markedly distinct (Supplementary Fig. S1B and S1C).

We next generated the GSC lines stably expressing the enhanced GFP (EGFP) under the *Nestin* promoter (GSCs-pE-Nes), activity of which reflects NSC properties (Fig. 1B; ref. 24). To examine how GSCs-pE-Nes lines differentiate in an *in vivo* environment over time, cells were inoculated in the brain of NOD/SCID mice (Fig. 1B). GSCs-pE-Nes outgrew rapidly and showed still high level of Nestin expression and almost no detectable level of GFAP (glial marker) expression after 1 week. GSCs-pE-Nes gradually converted into differentiated tumor cells, and after 4 weeks, the majority of GSCs-pE-Nes expressed GFAP, whereas the minority expressed Nestin in the tumors. Because the assays for CSC showed their potential for self-renewal, tumor propagation, and differentiation, our model seems to fit the CSC model (30).

We next examined whether serum exposure *in vitro* could also direct the progression of GSCs into differentiated tumor cells as was observed in the brain of NOD/SCID mice. Sphere-forming GSCs became adherent in response to serum within 48 hours and were termed S-BTCs. The expression levels of *CD133*, *Nestin*, and *Nanog* were reproducibly downregulated after continuous serum exposure (Fig. 1C and E and Supplementary Fig. S1E). In contrast, the expression of differentiation markers, *GFAP* and neuron-specific class III β-tubulin (neuronal marker, β III tubulin), was upregulated in S-BTCs as compared with the corresponding GSCs along with an attenuation of tumorigenicity in NOD/SCID mice as reported previously (Fig. 1D and E; Supplementary Table S2; ref. 5). Comparison of cell growth between GSCs and S-BTCs indicated that the attenuation of tumorigenicity in S-BTC was not simply because of reduced proliferation (Fig. 1F). These observations indicated that a unique feature of primary glioblastoma-derived GSCs in our model is their ability to initiate the differentiation program in response to environmental conditions (i.e., orthotopic site of NOD/SCID mice or serum exposure), via downregulation of *Nanog* and other pluripotency-related genes and induction of the differentiation-related genes in S-BTCs (31).

Bidirectional interconvertibility between GSCs and S-BTCs

Although the possibility of bidirectional interconvertibility between CSCs and non-CSCs has been mentioned, it has been little explored (8, 9). In our GSC model, we found that if the serum was withdrawn in the S-BTC culture after 3 weeks of continuous exposure, tumor cells reformed spheroids again (revertant-GSCs, Rev-GSCs; Fig. 2A). It is possible that this simply reflected clonal selection of minor populations, in which "unresponsive-GSCs" maintain GSC characteristics in serum conditions and may contribute to reforming spheres following return to NBE. However, via limiting dilution analysis, more than half of S-BTCs have the capability of reconverting into GSCs (see Materials and Methods). Consistent with the morphologic interconversion between GSCs and S-BTCs, intrinsic neural stem cell marker profiles were found in these Rev-GSCs (Fig. 2B and Supplementary Fig. S1D). Furthermore, GSCs-pE-Nes lost the EGFP expression by 96 hours in serum-containing culture and reexpressed EGFP following return to NBE for 72 hours (Fig. 2C). This reversible *Nestin* promoter activity retained until medium change at 3 to 4 weeks. More importantly, in contrast to the attenuated tumorigenicity of S-BTCs, Rev-GSCs recovered high tumorigenicity capabilities in the brain of NOD/SCID mice, indicating that conversion of GSCs to S-BTCs is functionally plastic and reversible within a certain period of time (Supplementary Table S2).

Epigenetic silencing mediated by PRC2-H3K27me3 in GSCs

Because *Nanog* expression displayed the best correlation with plastic interconversion among the pluripotency-related markers, being consistently downregulated in response to serum, we examined how epigenetic mechanisms affected *Nanog* expression (Fig. 3A). Although DNA methylation of this gene was not altered and seemed not to be involved in this silencing process, H3K27me3 on the *Nanog* promoter was approximately 3-fold enriched after serum addition to GSCs. Downregulation of EZH2 via a shRNA knockdown system (EZH2-KD; Supplementary Fig. S2A) in GSCs suppressed enrichment of H3K27me3 at the *Nanog* promoter after serum exposure, which resulted in sustained expression of *Nanog* (Fig. 3A and B). This derepression of *Nanog* by EZH2-KD was rescued by exogenous expression of an shRNA-insensitive EZH2 (EZH2-exp), in which the target site of shRNA was mutated (Fig. 3B).

Intriguingly, subcellular localization of EZH2 seemed to be associated with morphologic conversion of GSCs in response to serum, although the expression level of EZH2 was not remarkably different between GSCs and S-BTCs (Fig. 3C–E and Supplementary Fig. S1F). Immunofluorescence analysis revealed that EZH2 was localized in both the nucleus and cytoplasm of GSCs. After serum exposure, it translocated primarily into the nucleus of more than 50% of the cells within 24 to 48 hours and subsequently retracted into the cytoplasm by 72 hours (Fig. 3C and D). The amount of EZH2 in the cytosolic and nuclear fractions as assessed by Western blotting seemed to parallel the observations in the immunofluorescence images (Fig. 3E). Other components of PRC2, such as EED and SUZ12, also behaved similarly to EZH2, suggesting that these PRC2 components work together in the nucleus (Supplementary Fig. S2B and S2C). Consistently, we found that exogenous expression of the shRNA-insensitive EZH2 lacking nuclear localization sequence (EZH2-dNLS), which localized predominantly in the cytosol (25), failed to rescue the derepression of *Nanog* in GSCs after serum exposure (Fig. 3B). These data indicated that dynamic translocation of PRC2 during the phenotypic conversion of GSCs played an important

Published OnlineFirst May 29, 2013; DOI: 10.1158/0008-5472.CAN-13-0109

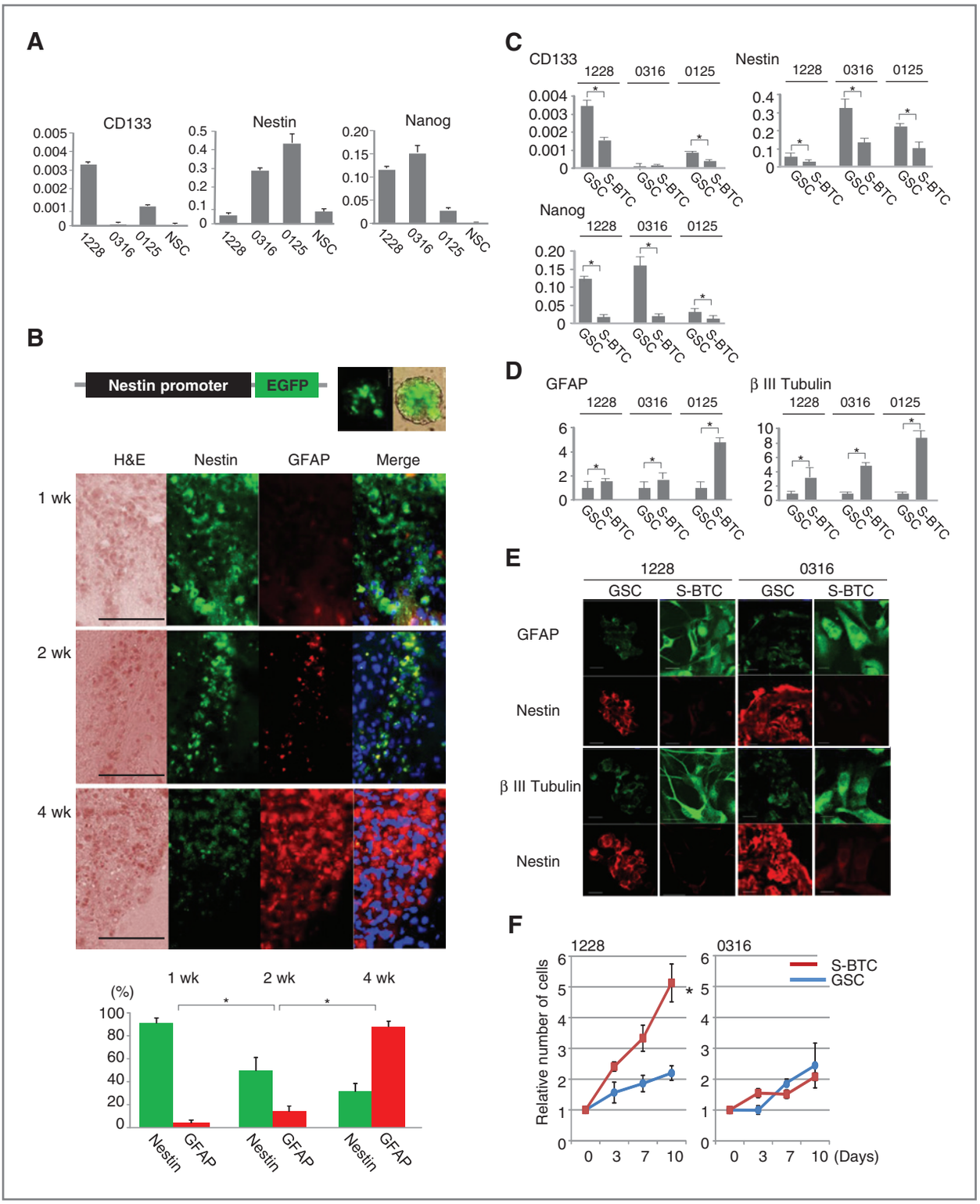

Figure 1. Phenotypic change of glioma-stem cells in *in vivo* and in serum. A, mRNA expression of stem cell markers (*CD133* and *Nestin*) and pluripotency-related marker (*Nanog*) in GSCs and NSCs. *Y*-axis indicates relative expression ratio of target mRNA/GAPDH mRNA. B, GSC lines stably expressing the EGFP under the *Nestin* promoter (top) in the brain of mice (middle). More than 50% of the cells in the spheres expressed high level of EGFP (top, right). Percentage of Nestin- and GFAP-positive cells in 4 different high-power fields (bottom; mean ± SD). *, $P < 0.05$. Blue, 4′,6-diamidino-2-phenylindole (DAPI) staining. Bar, 50 μm. mRNA expression (mean ± SD) of *CD133*, *Nestin*, and *Nanog* (C) and differentiation markers (*GFAP* and *β III tubulin*, D) in GSCs and S-BTCs. *, $P < 0.05$. E, immunofluorescence of GSCs and S-BTSCs (3 weeks after serum exposure) with GFAP, β III tubulin, and Nestin. Bar, 20 μm. F, *in vitro* cell growth of GSCs and S-BTCs (mean ± SD). *, $P < 0.05$.

Published OnlineFirst May 29, 2013; DOI: 10.1158/0008-5472.CAN-13-0109

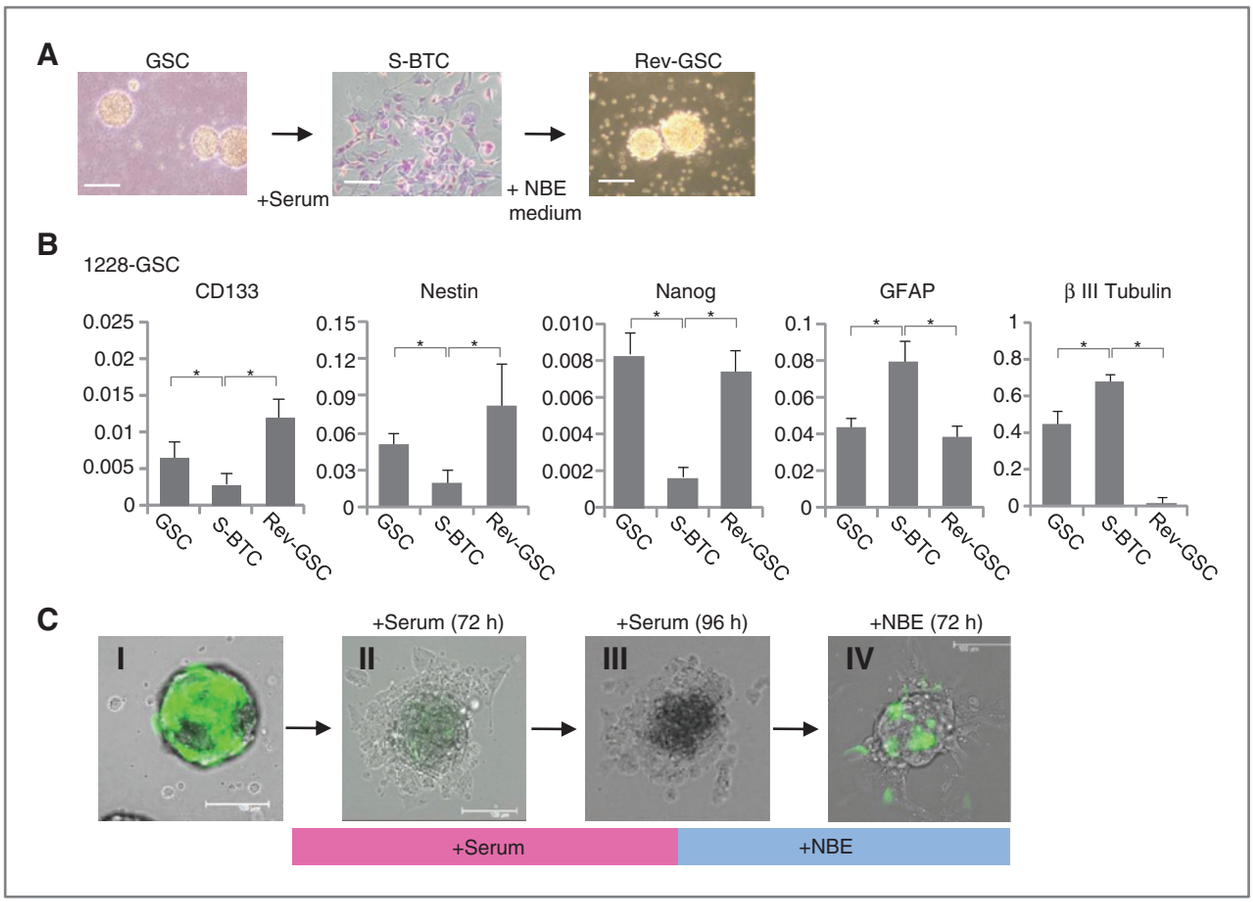

Figure 2. Interconvertibility between GSCs and S-BTCs. A, phase contrast images of 1228-GSCs, revertant GSCs (Rev-GSC), and S-BTC stained with crystal violet. Bar, 50 μm. B, mRNA expression (mean ± SD) of indicated genes in 1228-GSCs, S-BTCs, and Rev-GSCs. Relative values of mRNA expression for each gene to GAPDH are shown on the *y*-axis. *, $P < 0.05$. C, convertible *Nestin* promoter activity in 1228-GSCs-pE-Nes. 1228-GSCs-pE-Nes lost the EGFP expression by 96 hours in serum-containing culture and reexpressed EGFP following return to NBE for 72 hours. Bar, 100 μm.

role in epigenetic reprogramming of H3K27me3-repressive mark in certain loci, such as *Nanog*.

Depletion of EZH2 suppresses interconversion of GSCs and S-BTCs

Next, we investigated the effect of inhibition of EZH2 on GSC conversion. EZH2-KD attenuated the ability of GSCs to differentiate into S-BTC in response to serum, in contrast to control GSCs (Fig. 3F). Attenuated GSC conversion by EZH2-KD was rescued by exogenous expression of EZH2-exp, whereas EZH2-dNLS failed to rescue it in GSCs after serum exposure (Supplementary Fig. S1G). These results were supported by the findings showing the effects of a potent PRC2 inhibitor, DZNep, on GSCs (32). Although DZNep affects multiple methyltransferases via inhibition of S-adenosylhomocysteine hydrolase, it preferentially disrupts the PRC2 activity. Global gene expression analysis revealed that the DZNep-mediated profile change was significantly correlated with EZH2-KD-mediated changes in 1228-GSCs ($P < 0.001$; Supplementary Fig. S2D), suggesting that pharmacologic inhibition of PRC2 by this compound results in the elimination of EZH2 and other PRC2 components from the target loci. Expression profiles analyzed by PCA revealed that GSCs with DZNep treatment in the serum condition more closely resembled the original GSCs than S-BTCs (Supplementary Fig. S2E). DZNep-treated cells retained a spheroid shape with high Nestin expression but no GFAP expression after serum exposure (Fig. 3G). Of note, DZNep also inhibited the conversion of S-BTCs to Rev-GSCs after withdrawal of serum (Fig. 3H). Thus, EZH2 depletion/inhibition impaired the bidirectional conversion between GSCs and S-BTCs, indicating that a switch from an active to silent state of particular gene sets regulated by PRC2-H3K27me3 in each cell type might be a key mechanism underlying the phenotypic plasticity observed.

Global analyses of the genes regulated by PRC2-mediated H3K27me3 and DNA methylation in GSCs and S-BTCs

To decipher the global target genes of PRC2-mediated H3K27me3 in the process of interconversion, we conducted ChIP microarray (ChIP-chip) analysis on GSCs and S-BTCs. Initial validation of our ChIP-chip analysis is described in Supplementary Fig. S3 and Supplementary Table S3. Of note, 217, 1,024, and 1,525 genes in 1228-GSCs, 0316-GSCs, and 0125-GSCs, respectively, showed enrichment of H3K27me3 (Fig. 4A; Supplementary Fig. S3A–S3C; Supplementary Table S4). During

Published OnlineFirst May 29, 2013; DOI: 10.1158/0008-5472.CAN-13-0109

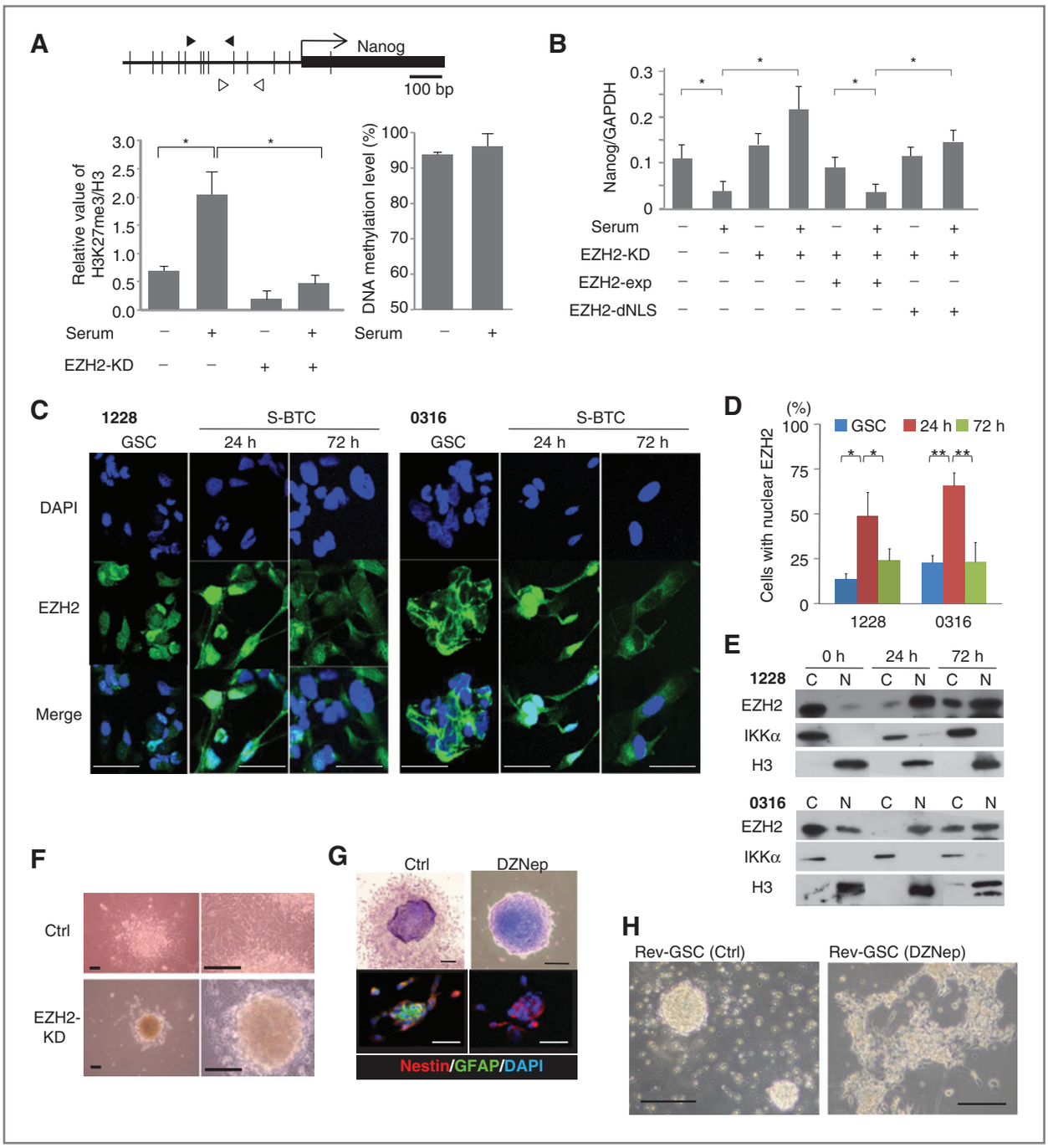

Figure 3. Association of EZH2 with phenotypic conversion of GSCs and S-BTCs. A, the transcription start site (arrow) and location of exon 1 (black box) of *Nanog* gene are indicated (top column). Open and closed arrowheads indicate the locations of ChIP-PCR and pyrosequencing primers, respectively. Vertical lines indicate CpG sites. Enrichment of H3K27me3 (relative value of H3K27me3 to H3, left) and DNA methylation level (right) at the *Nanog* promoter in 1228-GSCs and S-BTCs with or without shRNA against *EZH2* (EZH2-KD) infection are shown (bottom column). Error bars denote SDs from triplicate experiments. *, $P < 0.05$. B, *Nanog* mRNA expression (mean ± SD) in Ctrl-GSC and EZH2-KD GSCs, an shRNA-insensitive EZH2 (EZH2-exp) or an shRNA-insensitive EZH2 lacking nuclear localization sequence (EZH2-dNLS) with and without serum. *, $P < 0.05$. C, confocal immunofluorescence study to evaluate the localization of EZH2 in GSCs incubated in NBE medium and S-BTCs after serum exposure. Bar, 20 μm. D, percentage of prominent EZH2-immunoreactive cells in the nucleus. Mean ± SD of four different high-power fields. *, $P < 0.05$; **, $P < 0.01$. E, Western blot analysis of EZH2 in the cytosolic (C) and nuclear (N) fractions of GSCs and S-BTCs at 0, 24, and 72 hours after serum exposure. IKKα and histone H3 are indicated as fractionated cytosolic and nuclear controls, respectively. F, phase contrast images of a control (Ctrl) sphere and an EZH2-KD sphere after serum exposure. Right, magnified images of left. Bar, 50 μm. G, phase contrast images of crystal violet staining (top; bar, 50 μm) and immunofluorescence images (bottom; bar, 10 μm) of GSCs with serum added (Ctrl) and 0316-GSCs treated with 5 μmol/L DZNep followed by serum addition (DZNep). H, phase contrast images of control revertant-GSCs converted from 1228-S-BTC (Ctrl) and revertant-GSCs converted from 1228-S-BTC treated with 5 μmol/L DZNep followed by withdrawal of serum (DZNep). Bar, 100 μm.

Published OnlineFirst May 29, 2013; DOI: 10.1158/0008-5472.CAN-13-0109

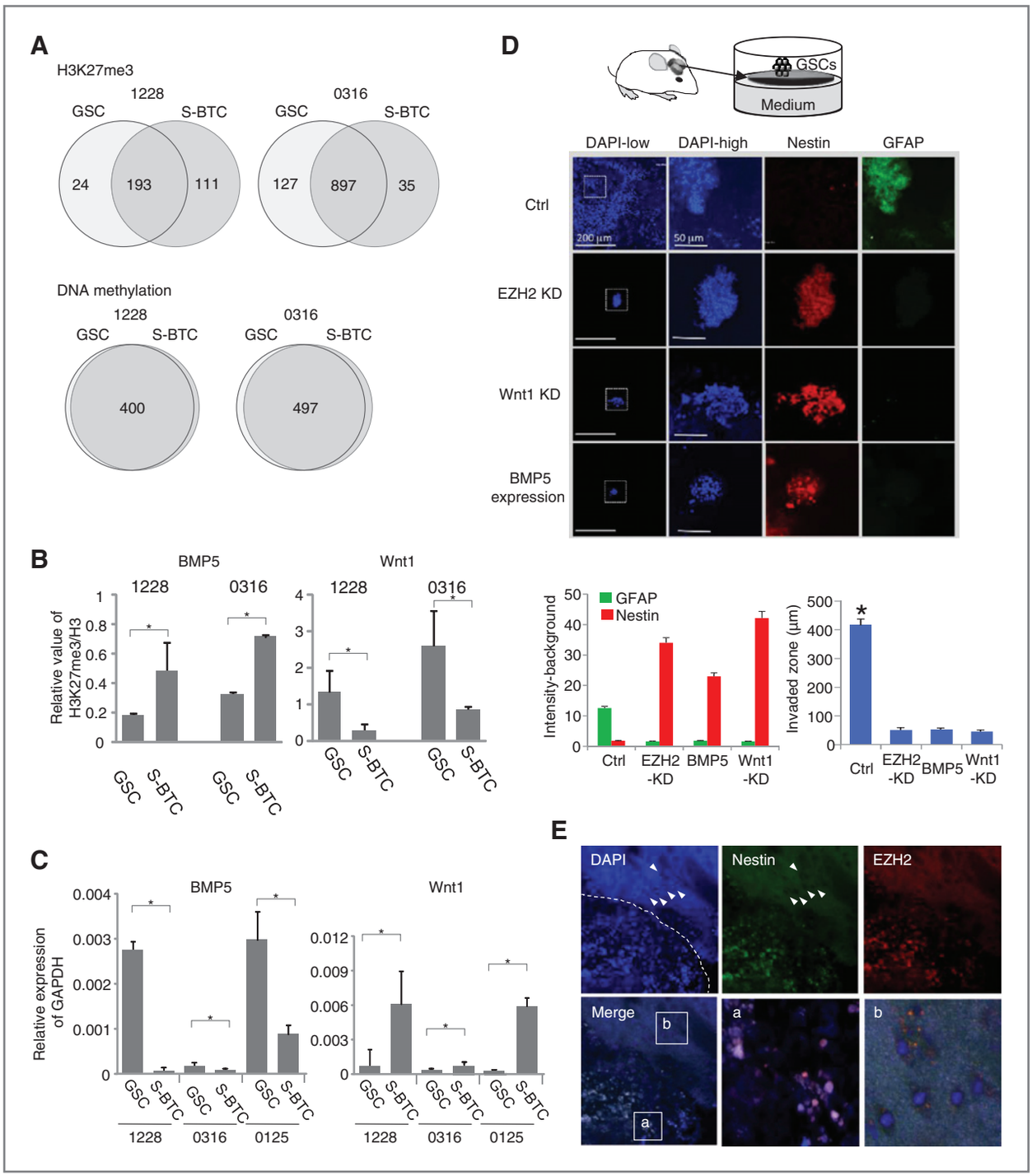

Figure 4. Targets of PRC2-mediated H3K27me3 based on global analyses in GSCs and S-BTCs. A, H3K27me3 targets in 1228-GSC, and 0316-GSC were assessed by a ChIP-chip analysis (top). DNA methylation targets compared in 1228-GSC and S-BTC, and 0316-GSC and S-BTC by MCAM analysis (bottom). B, H3K27me3 enrichment at *BMP5* and *Wnt1* promoters in GSCs and S-BTCs. The *y*-axis represents the same as Fig. 3A. *, $P < 0.05$. C, *BMP5* and *Wnt1* mRNA expression in GSCs and S-BTCs. *, $P < 0.05$. D, brain-slice assay. 1228-GSCs transduced with either mock control (Ctrl), EZH2-shRNA (EZH2-KD), Wnt1-shRNA (Wnt1-KD), or BMP5-overexpression (BMP5-expression) were placed in the basal ganglia of nude mouse for 14 days (top). Area within white rectangles in the 4′,6-diamidino-2-phenylindole (DAPI) images with low magnification (DAPI-low) are magnified as DAPI-high, Nestin, and GFAP (middle). The expression index of GFAP and Nestin was calculated (bottom, right). *Y*-axis indicates value of (intensity-background, mean ± SD) × region of interest. The ability of tumor cell expansion was analyzed by invaded zone (bottom, right). *Y*-axis indicates maximum diameter of anchored area (DAPI-positive invasion area). *, $P < 0.05$. E, 1228-GSCs-pE-Nes were cultured for 7 days on mouse brain slice. Dashed line, border of sphere. Arrowheads, differentiated tumor cells spread into the surrounding brain tissue. The areas labeled a and b in the merged image (bottom left) are magnified in a and b. Bar, 50 μm.

Published OnlineFirst May 29, 2013; DOI: 10.1158/0008-5472.CAN-13-0109

the conversion of GSCs to S-BTCs, both gain and loss of H3K27me3 marks were found in 1228-GSCs and 0316-GSCs (Fig. 4A and Supplementary Table S4). Comparison of ChIP-chip and gene expression array analyses during this process revealed that genes with H3K27me3 enrichment were significantly downregulated in both GSC lines ($P = 4.5 \times 10^{-7}$ in 1228-GSCs and -S-BTCs, and $P = 5.4 \times 10^{-9}$ in 0316-GSCs and -S-BTCs; based on χ^2 test), indicating that these epigenetic alterations reflect and likely mediate gene expression (Supplementary Table S5).

In contrast, patterns of DNA methylation were remarkably stable after continuous exposure to serum for a month. Initial validation of the MCAM analysis is described in Supplementary Fig. S3D and Supplementary Table S3. Global analysis of promoter CpG island DNA methylation status showed no reproducible differences between GSCs and S-BTCs over 1 month (Fig. 4A).

BMP5 and *Wnt1* are the targets of PRC2-mediated H3K27me3 in the process of interconversion

Among the H3K27me3 target genes, GSCs gained H3K27me3 at the *BMP5* promoter and lost H3K27me3 at the *Wnt1* promoter during the conversion to S-BTCs. The expression of these genes was inversely correlated with alterations of H3K27me3 status in GSCs, suggesting that PRC2-mediated H3K27me3 regulates the interconversion of GSCs via switching of these target genes (Fig. 4B and C).

To further examine whether PRC2-mediated gene regulation is obligatory for the plasticity of GSCs during adaptation to surrounding environments, we applied an *ex vivo* brain tissue model, which was analogous to the physiologic environment (Fig. 4D; ref. 33). GSCs were transduced retrovirally with Wnt1-shRNA, EZH2-shRNA, or BMP5 (Supplementary Fig. S4A). The off-target effects of EZH2-shRNA and Wnt1-shRNA constructs were excluded using shRNA targeting different regions of the genes (Supplementary Fig. S4B–S4D). Control GSCs spread to and integrated into the surrounding brain tissue during 14 days while displaying increased expression of GFAP and decreased expression of Nestin, as observed in the *in vitro* cell culture system (Figs. 1E and 4D). In contrast, BMP5-overexressing GSCs, Wnt1-KD GSCs, and EZH2-KD GSCs retained spheroid morphology and failed to expand in brain tissues. Nestin expression was retained and GFAP expression was not induced in those manipulated cells. To evaluate the relationship between the initial adaptation of GSCs into the surrounding brain tissue and subcellular localization of EZH2, GSCs-pE-Nes were cultured for a short period (7 days) on mouse brain slice (Fig. 4E). GSCs-pE-Nes spread to and integrated into the surrounding brain tissue. Intriguingly, the remaining sphere-like tumor cells expressed EGFP under the control of the *Nestin* promoter and nuclear EZH2, whereas reduction of EGFP and cytoplasmic EZH2 were observed in spindle-shaped differentiated tumor cells spread in the brain parenchyma.

The growth of these transduced GSCs was not significantly different from the parent GSCs (Supplementary Fig. S4E). These data suggested that inhibition of EZH2 and dysregulation of associated H3K27me3 target genes in GSCs impaired their integration into surrounding environments and may prevent tumor mass formation.

Dysregulation of PRC2-mediated H3K27me3 and its target genes abrogates tumorigenicity

In the context of glioblastoma treatment, we evaluated the effects of EZH2-KD and DZNep on GSC growth (32, 34). Inhibition of EZH2 resulted in slight to moderate growth suppression, no significant effect on apoptosis (sub-G_1 fraction), as well as slightly decreased BrdUrd incorporation, in both 1228- and 0316-GSCs (Supplementary Fig. S5).

Antitumorigenic effects by EZH2 depletion/inhibition were also confirmed in an orthotopic mouse model. Furthermore, Wnt1 depletion and BMP5 overexpression also markedly attenuated tumorigenicity (Supplementary Fig. S5I). It is plausible that the antitumorigenic effects of EZH2 depletion/inhibition may be due to their defective self-renewal potential, as it has been previously shown that EZH2 contributes to the self-renewal of GSCs (6, 34). However, given the above experimental evidence obtained with *in vivo*, *in vitro*, and *ex vivo* analyses, dysregulation of EZH2 and its associated genes may decrease the tumorigenicity of GSCs not only by defective self-renewal potential, but also by diminished plasticity, thereby suppressing GSC conversion into other cell types during adaptation to new environments.

Heterogeneous localization of EZH2 associated with glioblastoma cell differentiation

Our data showed that cancer cells usurp the PRC2-mediated H3K27me3 processes to mediate functional conversion in response to environmental cues, which was associated with subcellular localization of EZH2. Xenografts of GSCs in NOD/SCID mice showed regional variations in subcellular localization of EZH2 (Fig. 5A and B). In the tumor/normal brain border, certain populations of cells showed prominent nuclear localization of EZH2 together with high level of Nestin expression. In contrast, EZH2 was expressed in the cytoplasm of tumor cells in the core region of the tumor. Furthermore, the expression level of EZH2 in the tumor periphery seems to be slightly higher than in the core region, suggesting that the level of EZH2 might also be associated with tumor cell differentiation.

We next investigated the expression pattern of EZH2 in clinical glioblastoma tissues (Fig. 5C–F). EZH2 levels were abnormally elevated in gliomas as compared with normal brain tissues, with higher expression correlating with tumor grade (Supplementary Fig. S2F). Notably, localization of EZH2 was highly heterogeneous in glioblastomas (Fig. 5D–F). In particular, the number of tumor cells with nuclear EZH2 was larger around tumor vessels and at the invasion front as compared with other tumor sites in which tumor cells with cytoplasmic EZH2 were dominant, suggesting that nuclear EZH2 may be involved in the process of reprogramming the tumor cells that are in close proximity to surrounding environmental factors. A double-labeling confocal image showed nuclear localization of EZH2 in certain cells (around the tumor vessel), and cytoplasmic colocalization of EZH2 and GFAP in other cells, particularly in seemingly differentiated tumor cells (Fig. 5E and F). Thus, rather than a simple association of high EZH2 expression with more aggressive forms, subcellular location of EZH2 may play a role in tumor heterogeneity and tumor cell differentiation regulated by PRC2-mediated epigenetic plasticity.

Published OnlineFirst May 29, 2013; DOI: 10.1158/0008-5472.CAN-13-0109

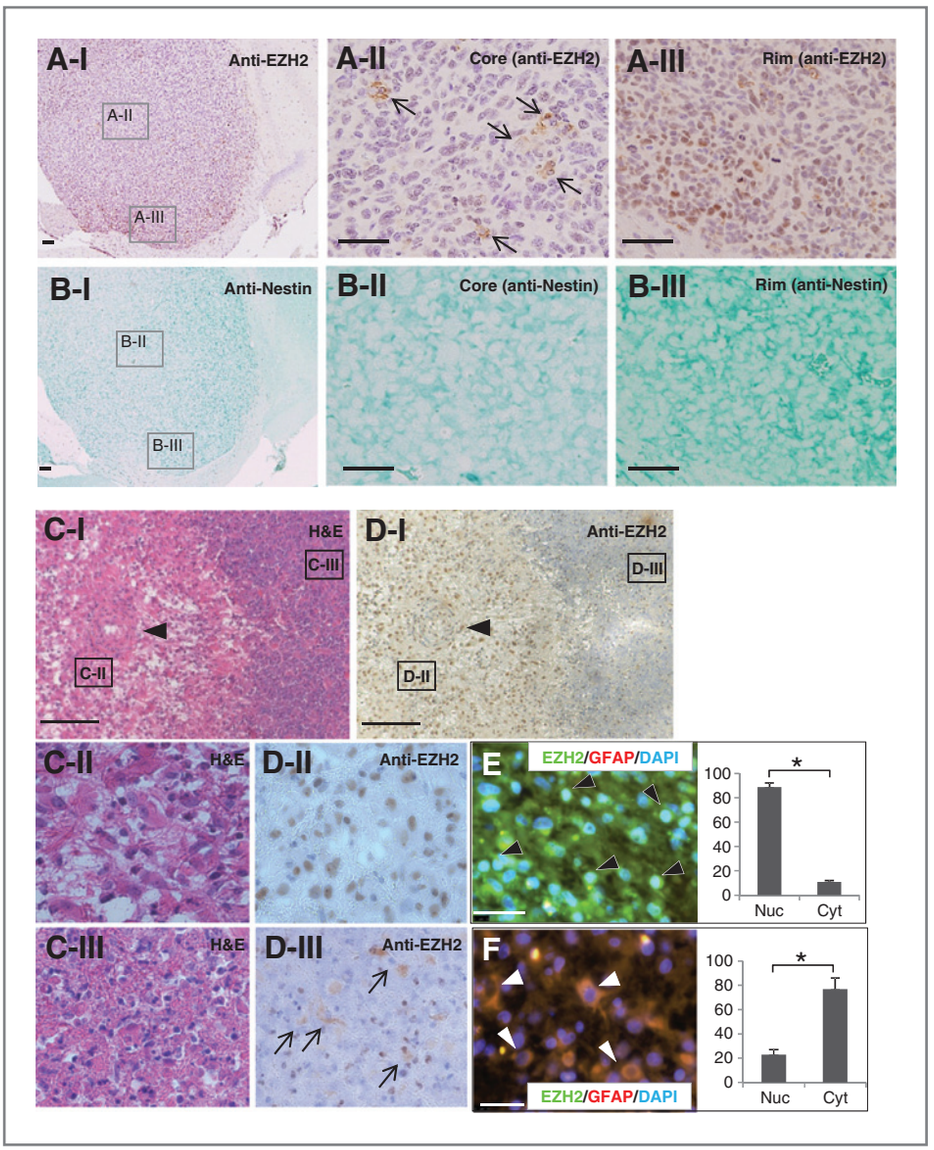

Figure 5. Heterogenous subcellular localization of EZH2 in a xenograft of GSCs in a NOD/SCID mouse and a clinical sample. A, immunohistochemistry of EZH2 in a 1228-GSC-derived xenograft. Two areas in A-I are magnified in A-II and A-III. Arrows indicate dominant expression of EZH2 in the cytoplasm. Bar, 50 μm. B, immunohistochemistry of Nestin in an adjacent section to A. Two areas in B-I are magnified in B-II and B-III. Bar, 50 μm. C, hematoxylin and eosin (H&E) staining of human glioblastoma section. The arrowhead indicates a tumor vessel. Bar, 200 μm. The areas (around the tumor vessel; C-II) and C-III in C-I are magnified in C-II and C-III. D, immunohistochemistry of EZH2 in an adjacent section to C. The arrowhead indicates a tumor vessel. Arrows indicate dominant expression of EZH2 in the cytoplasm. Bar, 200 μm. The areas (around the tumor vessel; D-II) and D-III in D-I are magnified in D-II and D-III. E and F, immunofluorescence study to evaluate the localization of EZH2 (green) and GFAP (red) in tumor cells around D-II and D-III. Cells are also stained with 4′,6-diamidino-2-phenylindole (DAPI) to highlight nuclear areas. Black triangles, representation of nuclear localization of EZH2; white triangles, representation of cytoplasmic colocalization of EZH2 and GFAP. Cells with nuclear (Nuc) and cytoplasmic (Cyt) EZH2 were counted in 3 views (50 cells in each view; right). Data are expressed as mean ± SD. *, $P < 0.05$. Bar, 25 μm.

Discussion

In the current study, we showed that tumor differentiation was associated with plastic epigenetic program that involves the dynamic loss and acquisition of histone marks as recently shown in melanoma (35). Phenotypic plasticity may exist between CSCs and non-CSCs within tumors (8, 36), which was invariably impaired by genetic knockdown or pharmacologic inhibition of the enzymatic components of PRC2. In response to extrinsic cues, the PRC2-mediated H3K27me3 gene silencing machinery seems to be a critical mediator of cancer-initiating cell plasticity via switching of target genes to adapt the tumor cells to their environment.

Recent studies showed that PRC2 not only acts to promote self-renewal, but also controls fate choices within the multipotent lineage in neural and muscle development (17–20, 37, 38). In addition to the normal cell differentiation, we recently showed that PRC2-mediated H3K27me3 regulatory pathways of miR-1275 may contribute to the tissue heterogeneity in glioblastomas (22).

The dynamic enrichment of the H3K27me3-repressive mark at the *Nanog* promoter locus was significantly detected in parallel with the downregulation of *Nanog* in S-BTCs, which functions as a key regulator for sustaining pluripotency (39). This repression of *Nanog* was closely associated with subcellular localization of EZH2/PRC2 in GSCs, indicating that dynamic translocation of EZH2/PRC2 during the phenotypic conversion of GSCs played an important role in epigenetic reprogramming. In addition to *Nanog*, we found that multiple GSC lines commonly showed altered expression of *BMP5*, a TGF-β family protein, and *Wnt1*, which seemed to be the targets of EZH2/PRC2, during the conversion. This is consistent with several studies showing that *BMP* or *Wnt* family genes are involved in maintaining stemness or stem cell differentiation (1, 2, 6, 7). Although activation of the Wnt pathway is

involved in stage-dependent regulation of neural precursor cell fate, a functional cross-talk exists between TGF-β and Wnt signaling in controlling the fate of neural stem cells switch from non-neurogenic cell division to differentiation (40, 41). Knockdown of EZH2 or Wnt1, overexpression of BMP5, or pharmacologic inhibition of EZH2 decreased plasticity of GSCs and impaired integration of GSCs into the brain parenchyma. Thus, in addition to PRC2-mediated regulatory mechanisms of stemness functions (42–44), we found here the novel aspect of EZH2/PRC2 in tumorigenesis; plastic epigenetic regulation by EZH2/PRC2 may confer tissue cell plasticity to GSCs to adapt to the microenvironment, which may explain the formation of tissue heterogeneity.

EZH2 expression was previously found to be elevated in several aggressive cancers (45, 46). Studies of pancreatic and breast cancers showed that nuclear accumulation of EZH2 is strongly associated with poor differentiation of cancers (47, 48). Rather than a proof that EZH2 is antioncogenic, we showed prominent levels of intratumoral heterogeneous EZH2 expression in glioblastoma. Immunofluorescence analysis revealed that around tumor vessels and at the invasion front where tumor cells were in close proximity to surrounding environmental factors, there was dominant localization of EZH2 in the nucleus. In contrast, substantial colocalization of both EZH2 and GFAP in the cytoplasm was observed in more differentiated tumor cells. These consistencies between EZH2 subcellular localization and tumor differentiation suggest that PRC2-mediated epigenetic plasticity in glioblastoma contributes to intratumoral heterogeneity. In a mouse model, cytosolic Ezh2 was found to control cellular signaling via its methyltransferase activity (25). Although the precise roles of cytosolic EZH2 in glioblastoma cells are not clear, our data suggest that the dynamic shift in the localization of EZH2 is fundamentally linked to tumor cell differentiation.

Thus, our data convincingly showed that the phenotypic interconversion between GSCs and S-BTCs is controlled by the H3K27 methylation status that is mediated by EZH2. However, these two states may not be simply regarded as representing the stem- and non-stem glioma cells, as S-BTC status may still contain a certain population of "stem cells" and *vice versa*. We still need further studies to clarify the precise regulatory mechanisms of CSC plasticity.

Part of the CSC hypothesis stipulates that aberrant self-renewal may be a mechanism that mediates tumorigenicity/recurrence by replenishing the CSC pool; therefore, developing CSC-specific therapies should be required. However, our data showed that interconversion between GSCs and non-GSCs exist, which may raise the possibility that therapeutic elimination of CSCs is followed by their regeneration from residual non-CSCs, allowing tumor regrowth and clinical relapse (8). Inhibition of EZH2 activity abrogates plasticity and eliminates tumorigenesis in an orthotopic model. Intratumoral heterogeneity is linked to therapeutic resistance, tumor recurrence, and metastatic progression. Further considerations are needed to translate our observations into clinical therapy, as the current study was conducted in an xenograft model in which the implanted tissue was not native to human glioma cells. Nevertheless, our data provide important new insights into molecular mechanisms for brain tumorigenesis that may be relevant to other neoplasms. Targeting plasticity may provide a new paradigm in cancer treatment.

Disclosure of Potential Conflicts of Interest

H. Okano is employed as SAB in San Bio Inc. and has ownership interest (including patents) in stocks of San Bio Inc. and patents on stem cells. No potential conflicts of interest were disclosed by the other authors.

Authors' Contributions

Conception and design: A. Natsume, M. Ito, K. Katsushima, Y. Kondo
Development of methodology: K. Katsushima, F. Ohka, M. Uesugi, Y. Kondo
Acquisition of data (provided animals, acquired and managed patients, provided facilities, etc.): M. Ito, A. Hatanaka, K. Shinjo, S. Sato, S. Takahashi, Y. Ishikawa, Y. Kondo
Analysis and interpretation of data (e.g., statistical analysis, biostatistics, computational analysis): A. Natsume, M. Ito, K. Katsushima, F. Ohka, A. Hatanaka, K. Shinjo, S. Sato, I. Takeuchi, Y. Kondo
Writing, review, and/or revision of the manuscript: A. Natsume, J.-P.J. Issa, Y. Sekido, Y. Kondo
Administrative, technical, or material support (i.e., reporting or organizing data, constructing databases): H. Shimogawa, H. Okano, S.U. Kim, T. Wakabayashi, Y. Kondo
Study supervision: M. Uesugi, J.-P.J. Issa, Y. Sekido, Y. Kondo

Acknowledgments

The authors thank Ikuko Tomimatsu, Hidenori Yokoyama, Daiki Ito, Takenori Kato, and Kanako Yuki for their technical assistance.

Grant Support

This work was supported by grant from PRESTO of JST (Y. Kondo; 4219), Grant-in-Aid for Scientific Research from the Japan Society for the Promotion of Science (Y. Kondo, 23300344; A. Natsume, 24390341), the Uehara Memorial Foundation (Y. Kondo), and Takeda Science Foundation (Y. Kondo).

The costs of publication of this article were defrayed in part by the payment of page charges. This article must therefore be hereby marked *advertisement* in accordance with 18 U.S.C. Section 1734 solely to indicate this fact.

Received January 12, 2013; revised April 16, 2013; accepted May 6, 2013; published OnlineFirst May 29, 2013.

References

1. Polyak K, Weinberg RA. Transitions between epithelial and mesenchymal states: acquisition of malignant and stem cell traits. Nat Rev Cancer 2009;9:265–73.
2. Reya T, Morrison SJ, Clarke MF, Weissman IL. Stem cells, cancer, and cancer stem cells. Nature 2001;414:105–11.
3. Chen J, Li Y, Yu TS, McKay RM, Burns DK, Kernie SG, et al. A restricted cell population propagates glioblastoma growth after chemotherapy. Nature 2012;488:522–6.
4. Singh SK, Hawkins C, Clarke ID, Squire JA, Bayani J, Hide T, et al. Identification of human brain tumour initiating cells. Nature 2004;432:396–401.
5. Lee J, Kotliarova S, Kotliarov Y, Li A, Su Q, Donin NM, et al. Tumor stem cells derived from glioblastomas cultured in bFGF and EGF more closely mirror the phenotype and genotype of primary tumors than do serum-cultured cell lines. Cancer Cell 2006;9:391–403.
6. Lee J, Son MJ, Woolard K, Donin NM, Li A, Cheng CH, et al. Epigenetic-mediated dysfunction of the bone morphogenetic protein pathway inhibits differentiation of glioblastoma-initiating cells. Cancer Cell 2008;13:69–80.
7. Penuelas S, Anido J, Prieto-Sanchez RM, Folch G, Barba I, Cuartas I, et al. TGF-beta increases glioma-initiating cell self-renewal through the induction of LIF in human glioblastoma. Cancer Cell 2009;15:315–27.

Published OnlineFirst May 29, 2013; DOI: 10.1158/0008-5472.CAN-13-0109

8. Gupta PB, Chaffer CL, Weinberg RA. Cancer stem cells: mirage or reality? Nat Med 2009;15:1010–2.
9. Gupta PB, Fillmore CM, Jiang G, Shapira SD, Tao K, Kuperwasser C, et al. Stochastic state transitions give rise to phenotypic equilibrium in populations of cancer cells. Cell 2011;146:633–44.
10. Jones PA, Baylin SB. The fundamental role of epigenetic events in cancer. Nat Rev Genet 2002;3:415–28.
11. Cadieux B, Ching TT, VandenBerg SR, Costello JF. Genome-wide hypomethylation in human glioblastomas associated with specific copy number alteration, methylenetetrahydrofolate reductase allele status, and increased proliferation. Cancer Res 2006;66:8469–76.
12. Bracken AP, Helin K. Polycomb group proteins: navigators of lineage pathways led astray in cancer. Nat Rev Cancer 2009;9:773–84.
13. Kondo Y, Shen L, Yan PS, Huang TH, Issa JP. Chromatin immunoprecipitation microarrays for identification of genes silenced by histone H3 lysine 9 methylation. Proc Natl Acad Sci U S A 2004;101:7398–403.
14. Sparmann A, van Lohuizen M. Polycomb silencers control cell fate, development and cancer. Nat Rev Cancer 2006;6:846–56.
15. Kondo Y, Shen L, Cheng AS, Ahmed S, Boumber Y, Charo C, et al. Gene silencing in cancer by histone H3 lysine 27 trimethylation independent of promoter DNA methylation. Nat Genet 2008;40:741–50.
16. Cedar H, Bergman Y. Linking DNA methylation and histone modification: patterns and paradigms. Nat Rev Genet 2009;10:295–304.
17. Boyer LA, Plath K, Zeitlinger J, Brambrink T, Medeiros LA, Lee TI, et al. Polycomb complexes repress developmental regulators in murine embryonic stem cells. Nature 2006;441:349–53.
18. Lee TI, Jenner RG, Boyer LA, Guenther MG, Levine SS, Kumar RM, et al. Control of developmental regulators by polycomb in human embryonic stem cells. Cell 2006;125:301–13.
19. Azuara V, Perry P, Sauer S, Spivakov M, Jørgensen HF, John RM, et al. Chromatin signatures of pluripotent cell lines. Nat Cell Biol 2006;8:532–8.
20. Pereira JD, Sansom SN, Smith J, Dobenecker MW, Tarakhovsky A, Livesey FJ. Ezh2, the histone methyltransferase of PRC2, regulates the balance between self-renewal and differentiation in the cerebral cortex. Proc Natl Acad Sci U S A 2010;107:15957–62.
21. Yuki K, Natsume A, Yokoyama H, Kondo Y, Ohno M, Kato T, et al. Induction of oligodendrogenesis in glioblastoma-initiating cells by IFN-mediated activation of STAT3 signaling. Cancer Lett 2009;284:71–9.
22. Katsushima K, Shinjo K, Natsume A, Ohka F, Fujii M, Osada H, et al. Contribution of microRNA-1275 to Claudin11 protein suppression via a polycomb-mediated silencing mechanism in human glioma stem-like cells. J Biol Chem 2012;287:27396–406.
23. Kim SU. Human neural stem cells genetically modified for brain repair in neurological disorders. Neuropathology 2004;24:159–71.
24. Kawaguchi A, Miyata T, Sawamoto K, Takashita N, Murayama A, Akamatsu W, et al. Nestin-EGFP transgenic mice: visualization of the self-renewal and multipotency of CNS stem cells. Mol Cell Neurosci 2001;17:259–73.
25. Su IH, Dobenecker MW, Dickinson E, Oser M, Basavaraj A, Marqueron R, et al. Polycomb group protein ezh2 controls actin polymerization and cell signaling. Cell 2005;121:425–36.
26. Tseng CK, Marquez VE, Fuller RW, Goldstein BM, Haines DR, McPherson H, et al. Synthesis of 3-deazaneplanocin A, a powerful inhibitor of S-adenosylhomocysteine hydrolase with potent and selective *in vitro* and *in vivo* antiviral activities. J Med Chem 1989;32:1442–6.
27. Estecio MR, Yan PS, Ibrahim AE, Tellez CS, Shen L, Huang TH, et al. High-throughput methylation profiling by MCA coupled to CpG island microarray. Genome Res 2007;17:1529–36.
28. Shen L, Kondo Y, Guo Y, Zhang J, Zhang L, Ahmed S, et al. Genome-wide profiling of DNA methylation reveals a class of normally methylated CpG island promoters. PLoS Genet 2007;3:2023–36.
29. Gao W, Kondo Y, Shen L, Shimizu Y, Sano T, Yamao K, et al. Variable DNA methylation patterns associated with progression of disease in hepatocellular carcinomas. Carcinogenesis 2008;29:1901–10.
30. Clarke MF, Dick JE, Dirks PB, Eaves CJ, Jamieson CH, Jones DL, et al. Cancer stem cells—perspectives on current status and future directions: AACR Workshop on cancer stem cells. Cancer Res 2006;66:9339–44.
31. Friedmann-Morvinski D, Bushong EA, Ke E, Soda Y, Marumoto T, Singer O, et al. Dedifferentiation of neurons and astrocytes by oncogenes can induce gliomas in mice. Science 2012;338:1080–4.
32. Tan J, Yang X, Zhuang L, Jiang X, Chen W, Lee PL, et al. Pharmacologic disruption of polycomb-repressive complex 2-mediated gene repression selectively induces apoptosis in cancer cells. Genes Dev 2007;21:1050–63.
33. Ohnishi T, Matsumura H, Izumoto S, Hiraga S, Hayakawa T. A novel model of glioma cell invasion using organotypic brain slice culture. Cancer Res 1998;58:2935–40.
34. Suva ML, Riggi N, Janiszewska M, Radovanovic I, Provero P, Stehle JC, et al. EZH2 is essential for glioblastoma cancer stem cell maintenance. Cancer Res 2009;69:9211–8.
35. Roesch A, Fukunaga-Kalabis M, Schmidt EC, Zabierowski SE, Brafford PA, Vultur A, et al. A temporarily distinct subpopulation of slow-cycling melanoma cells is required for continuous tumor growth. Cell 2010;141:583–94.
36. Santisteban M, Reiman JM, Asiedu MK, Behrens MD, Nassar A, Kalli KR, et al. Immune-induced epithelial to mesenchymal transition *in vivo* generates breast cancer stem cells. Cancer Res 2009;69:2887–95.
37. Palacios D, Mozzetta C, Consalvi S, Caretti G, Saccone V, Proserpio V, et al. TNF/p38alpha/polycomb signaling to Pax7 locus in satellite cells links inflammation to the epigenetic control of muscle regeneration. Cell Stem Cell 2010;7:455–69.
38. Margueron R, Reinberg D. The polycomb complex PRC2 and its mark in life. Nature 2011;469:343–9.
39. Jaenisch R, Young R. Stem cells, the molecular circuitry of pluripotency and nuclear reprogramming. Cell 2008;132:567–82.
40. Hirabayashi Y, Gotoh Y. Epigenetic control of neural precursor cell fate during development. Nat Rev Neurosci 2010;11:377–88.
41. Chung S, Leung A, Han BS, Chang MY, Moon JI, Kim CH, et al. Wnt1-lmx1a forms a novel autoregulatory loop and controls midbrain dopaminergic differentiation synergistically with the SHH-FoxA2 pathway. Cell Stem Cell 2009;5:646–58.
42. Lessard J, Sauvageau G. Bmi-1 determines the proliferative capacity of normal and leukaemic stem cells. Nature 2003;423:255–60.
43. Park IK, Qian D, Kiel M, Becker MW, Pihalja M, Weissman IL, et al. Bmi-1 is required for maintenance of adult self-renewing haematopoietic stem cells. Nature 2003;423:302–5.
44. Molofsky AV, Pardal R, Iwashita T, Park IK, Clarke MF, Morrison SJ. Bmi-1 dependence distinguishes neural stem cell self-renewal from progenitor proliferation. Nature 2003;425:962–7.
45. Varambally S, Dhanasekaran SM, Zhou M, Barrette TR, Kumar-Sinha C, Sanda MG, et al. The polycomb group protein EZH2 is involved in progression of prostate cancer. Nature 2002;419:624–9.
46. Kleer CG, Cao Q, Varambally S, Shen R, Ota I, Tomlins SA, et al. EZH2 is a marker of aggressive breast cancer and promotes neoplastic transformation of breast epithelial cells. Proc Natl Acad Sci U S A 2003;100:11606–11.
47. Raaphorst FM, Meijer CJ, Fieret E, Blokzijl T, Mommers E, Buerger H, et al. Poorly differentiated breast carcinoma is associated with increased expression of the human polycomb group EZH2 gene. Neoplasia 2003;5:481–8.
48. Ougolkov AV, Bilim VN, Billadeau DD. Regulation of pancreatic tumor cell proliferation and chemoresistance by the histone methyltransferase enhancer of zeste homologue 2. Clin Cancer Res 2008;14:6790–6.

Published OnlineFirst May 29, 2013; DOI: 10.1158/0008-5472.CAN-13-0109

Cancer Research
The Journal of Cancer Research (1916–1930) | The American Journal of Cancer (1931–1940)

AACR American Association for Cancer Research

Chromatin Regulator PRC2 Is a Key Regulator of Epigenetic Plasticity in Glioblastoma

Atsushi Natsume, Motokazu Ito, Keisuke Katsushima, et al.

Cancer Res 2013;73:4559-4570. Published OnlineFirst May 29, 2013.